

Real-time Soft Robot 3D Proprioception via Deep Vision-based Sensing

Ruoyu Wang¹, Shiheng Wang^{1*}, Erdong Xiao^{1*}, Kshitij Jindal^{1*}, Wenzhen Yuan², Chen Feng^{1†}

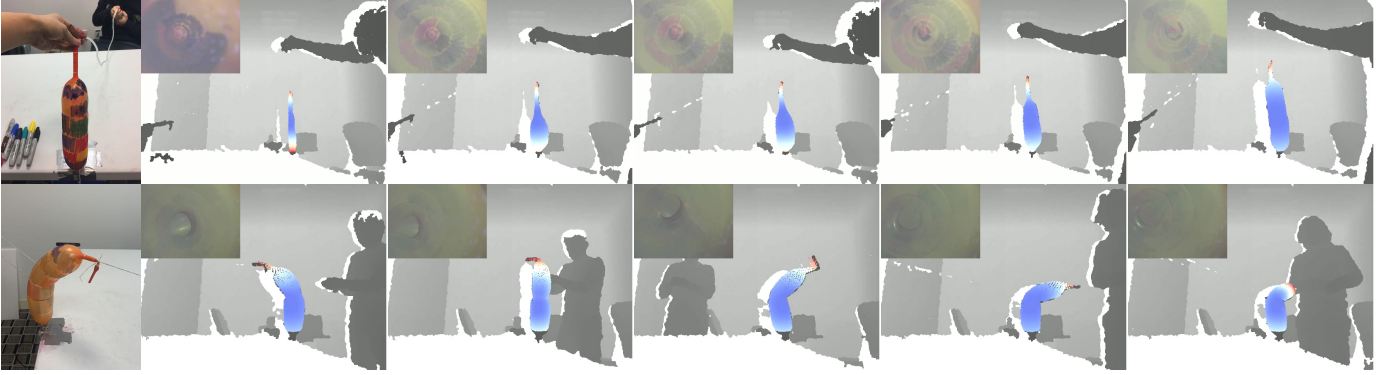


Fig. 1. Proprioception of a balloon soft robot using our vision-based sensing system, under expansion (top row) and bending (bottom row). We aim at predicting the real-time full 3D shapes of the robot, as rendered in the blue and red point clouds in the pictures (redder points indicate larger prediction error). The gray scale images are the depth image from an external Kinect sensor, and the top-left images are direct output from the embedded camera of the robot.

Abstract—The soft robots are welcomed in many robotic applications because of their high flexibility, which also poses a long-standing challenge on their proprioception, or measuring the real-time 3D shapes of the soft robots from internal sensors. The challenge exists in both the sensor design and robot modeling. In this paper, we propose a framework to measure the real-time high-resolution 3D shapes of soft robots. The framework is based on an embedded camera to capture the inside/outside patterns of the robots under different loading conditions, and a CNN to produce a latent code representing the robot state, which can then be used to reconstruct the 3D shape using a neural network improved from FoldingNet [1]. We tested the framework on four different soft actuators with various kinds of deformations, and achieved real-time computation ($<2\text{ms}/\text{frame}$) for robust shape estimation of high precision ($<5\%$ relative error for 2025 points) at an arbitrary resolution. We believe the method could be widely applied to different designs of soft robots for proprioception, and enabling people to better control them under complicated environments.

I. INTRODUCTION

Soft robots are built on soft materials or compliant mechanisms, and have very high degree-of-freedom regarding the configurations. A major advantage of the soft robots over the traditional rigid ones is compliance and flexibility. The soft robots can passively yield to the external physical contact, which makes them safe in contact-rich tasks. The infinite dimension of their shapes also enables them to fit complicated environments. Therefore, they show significant potentials to be applied to safety-related tasks, dexterous grasping and manipulation, and surgical applications. However, the high flexibility of soft robots poses extra challenges on the proprioception of soft robots, where the core tasks are to perceive the real-time

shapes of the robots. Compared to their rigid peers, soft robots are usually highly under-actuated and highly nonlinear, and external loads or contact will cause prominent deformation of the robots. The high-dimensional deformation can hardly be well measured by traditional sensors, and the representation of the high-dimensional shapes is also challenging. Without proper measurement and representation of soft robots' shape states, it is hard to perform closed-loop controls on those robots.

The present techniques for soft robot proprioception mostly use stretchable sensors to measure the local deformation on the robots [2, 3, 4]. Those sensors are resistive or capacitive sensors, and are built into the robot at the position that deformation is most likely to occur. However, the spatial sparsity design of this kind of sensors can hardly measure the high-dimensional deformation with the desired accuracy, and the manufacturing and the transformation to other soft robots are big challenges. Moreover, representing the high-dimensional 3D shapes of soft robots is challenging. A traditional practice is to use Finite Element Analysis (FEA) [5, 6], but the method has much constraints on the application conditions and requires huge computation resource, that making it impractical to run in real-time.

In this paper, we propose a framework to measure the real-time 3D deformation of soft robots using a data-driven method. We use an embedded camera to record the deformation of the internal patterns of the soft robots, and then train a Convolutional Neural Network (CNN) to encode the visual signals to a latent space for datasets involving complex motions, or directly down-sample and stretch the self-observing images to vectors for simpler motions, and then send the representation vectors to a decoder to recover 3D shapes of the soft robots. The network for 3D shape reconstruction runs in real-time on GPU, so that it can be used for closed-loop control and motion planning. Since the method is barely related to the hardware

¹ New York University, Brooklyn, NY 11201.

{ruoyuwang, sw4018, edxiao, kj1290, cfeng}@nyu.edu

² Stanford University, Stanford, CA, 94305. yuanwz@stanford.edu

* Equal contributions.

[†] The corresponding author is Chen Feng. cfeng@nyu.edu

design of the robots, it can be easily transformed on different soft robots.

To test our method, we experimented with four different soft robots: balloon actuator, elastomeric origami [7], PneuNets [8] and a fiber reinforcement actuator [9]. The balloon actuators can actively expand or shrink, and the PneuNets and fiber reinforcement actuator can actively bend. We painted random patterns in the robots, and mounted the cameras either inside or outside the robot body according to the robot design. We then collect datasets of more than 10,000 instances for each robot, which might be either active deformation or passive deformation caused by external force or contact. The datasets are used to train the neural networks for learning the representations of the robots' 3D shapes. To get the ground truth of the robots' shapes as complete as possible, we developed a dual RGBD camera system. The system can also be used in other research related to soft robots, and offer a low-cost solution of getting the ground truth shapes for the robots. Our experiment results (see Figure 1) show that this method can achieve high 3D shape sensing accuracy (absolute error: ≤ 5 mm, relative error: $\leq 5\%$, when the reconstruction resolution is 45×45 points) at any arbitrary reconstruction resolution in real-time computational speed ($\geq 450\text{Hz}$).

To our knowledge, the system proposed in this paper is the first vision-based methods for measuring the real-time 3D shapes of soft robots. The accuracy and spatial resolution of the measurement significantly surpass the ones using traditional methods. Since the method does not rely on the hardware design of the robots and cameras can be easily embedded, the method can be easily transformed to other soft robots, thus enabling soft robots to better perceive their real-time states, and perform closed-loop control in the complicated environments or for tasks that require more precise motion.

II. RELATED WORK

Soft robot proprioception. Traditionally, researchers embed stretchable sensors in the soft robots to measure local deformation. Those sensors include capacitive or resistive sensors that perform different electronic parameters under varied deformation conditions, and optical fibers whose light conductivity decreases during bending. Glauser et al. [10] use a capacitive sensor embedded in a soft robot and a multi-layer perceptron (MLP) to predict 3D positions of a set of key points from the capacitive readings. Van Meerbeek et al. [11] model a soft foam's state as a 2D vector of bend/twist angles, and use 30 optical fiber readings and K-Nearest-Neighbors/SVM/MLP models to learn the angles. Molnar et al. [12] also uses optical fibers as input to a 2-layer MLP for estimating the end-effector's 3D position of a linear soft pneumatic robot. For a more comprehensive summary of the existing measurement methods, we refer readers to [13]. A major limitation of those methods is that they are "over-simplified" [13] while trying to model the high-dimensional shapes of the soft robots with a low-dimensional vectors, thus compromise the accuracy and spatial resolution. The complicated driving conditions, where the robots are driven by multiple loads, will be challenging for

those sensors. This is caused by the intrinsic low resolution of the sensor components. Our method employs vision-based designs, which offer very rich high-resolution information regarding the high-dimensional deformation of the soft robots. The deep neural network models we developed then turns the raw readings into a full description of the 3D shapes of the robots. Our measuring method has low dependency to the robot design or the loading conditions, hence can be widely applied on different soft robots and to complicated working environments.

Vision-based sensors for soft bodies. Vision-based sensors have been designed in other areas to measure the shape of the soft bodies, like robot tactile sensing. Those sensors [14, 15, 16, 17], use a piece of soft material as the sensing medium, with some patterns painted on the surface or in the body, then use an embedded camera to track the deformation of the markers. Most of those sensors aim at measuring the contact force, but the deformation of the soft contact medium results in the direct measurement. Yuan et al. [18] introduce a similar sensor, but they also use the reflection from the soft material surface to reconstruct the high-resolution shape of the soft body. The successful practice of those sensors shows that vision-based sensor offers a convenient way to measure the deformation of soft materials, but compared to the soft robots that are studied in this work, those sensors only measures a small layer of the soft material, and the deformation is only on a plane. The deformation of the soft material is much larger and more complex in this work.

Reconstructing 3D shapes from images using neural networks. The computer vision community has been working on reconstructing 3D models from single images for several years. Works like [19], [20] and [21] focus on reconstructing the 3D models of commonly seen rigid objects. There are also works like [22] to reconstruct 3D human body structure, while the shapes are partially deformable. To reconstruct 3D shapes, up-convolutional (or transpose-convolutional) networks are often used [23]. The recent FoldingNet [1] provides another more light-weight and accurate possibility to reconstruct shapes as point clouds from deep parametric surfaces, thus being particularly suitable for representing soft robots' shapes. In this work, we also aim at reconstructing the 3D shapes from a single image using neural networks, but compared to those existing work where the images are external observation of the target object, our input data is from the internal view of the robots, and the intuitive correlation between the images and the shapes are much weaker.

III. REPRESENTATION LEARNING FOR SOFT ROBOTS

A. Overview

The proposed framework (Figure 2) has three main steps:

- **data collection:** images from the embedded camera are collected into a set $\mathcal{S} = \{\mathcal{S}_n\}$, and their corresponding 3D shapes are collected into a set $\hat{\mathcal{P}} = \{\hat{\mathcal{P}}_n\}$. Elements in \mathcal{S} and $\hat{\mathcal{P}}$ are paired up.
- **deep calibration:** A neural network is trained to model two-stage sensing functions $h_\psi : \mathcal{S} \rightarrow \mathbb{H}$ and $f_\theta : \mathbb{H} \rightarrow \mathbb{P}$,

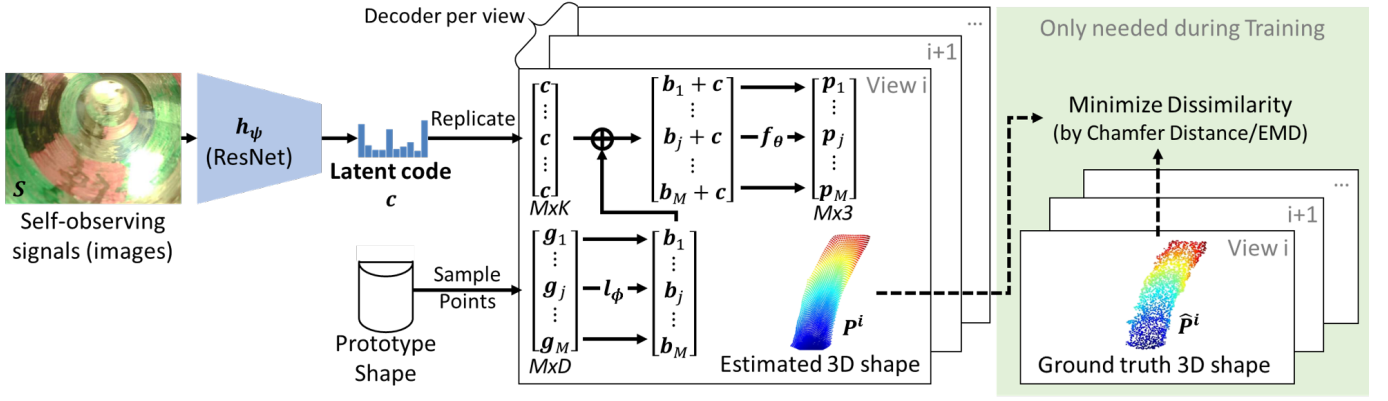


Fig. 2. **Algorithm pipeline.** Our network enables a generic soft robot perception framework. The network input is self-observing signals (in this paper, we use RGB images from the embedded camera), and the output is the estimated 3D shapes of the soft robot from different views, non-linearly “folded” from a rough prototype shape (a half cylinder) of the robot. Through training, a latent representation, the K -dimensional latent code, of the soft robot are automatically discovered, and enables a 3D shape estimation with high accuracy and arbitrary resolution. Solid arrows in the figure indicate forward propagation, and dashed arrows means loss calculation. \oplus means element-wise addition.

where \mathbb{H} is the latent space inside which a vector c represents a state of the soft robot. Note that \mathbb{H} can be a fixed down-sampling operator without learning, when the dataset only involves simple motions such as a bending soft finger. ψ and θ are learnable parameters. This process is analogous to the traditional sensor calibration with multiple inputs and outputs, so we name it as deep calibration.

- **deployment:** Using the learned functions, data-driven sensing can be performed by mapping current self-observed image S to the shape P without any on-the-fly fitting as required in NURBS-based methods [24].

With the development of deep learning, it is not difficult to find a proper encoder h_ψ depending on the self-observing sensors. For instance, CNN can be used for cameras, MLP for sensor arrays, and graph convolutional networks (GCN) for sensor networks. However, the decoder f_θ could only be 3D up-convolutional networks [23] or point cloud decoders, because our goal is to sense the 3D shape of soft robots, which is essential for follow-up tasks like control and motion planning. Considering the computational efficiency for robotic applications, we propose to use point cloud decoders rather than 3D up-convolutional networks. Because point cloud is a more concise representation of 3D shape, while voxels (used in 3D up-convolutional networks) naturally have the trade-off between memory/computation and shape resolution. Besides, point clouds consists of 3D coordinates directly, which can be readily used in tasks such as motion planning.

Among existing point cloud decoders, FoldingNet [1] provides the state-of-art point cloud decoder, which supports to decode an arbitrary number of points, providing theoretically infinite 3D shape resolutions for soft robots. Thus we choose to take advantage of FoldingNet-like 3D shape decoders.

B. Network Architecture

The original FoldingNet provides an auto-encoder architecture for point clouds. It uses PointNet[25] as its encoder and

a share-weight MLP as its decoder. The PointNet encodes a point cloud $\hat{P} = \{\hat{p}_i\}$ with N points into a code word c in a K dimensional latent space, then the code word is replicated for M times as $\mathbb{1}_M c$ ($\mathbb{1}_M$ is a M -dimensional column vector with all entries being one), and concatenated to a D -dimension point grid $G = [g_j]$. M can be chosen according to any desired decoding resolution even after training. After that, the $M \times (D + K)$ intermediate variable $[G, \mathbb{1}_M c]$ is fed to a share-weight MLP (weights shared across points) to obtain the decoded $M \times 3$ point cloud as $P = [p_j]$.

Mathematically, the original FoldingNet decoder realizes the following point-wise decoding function:

$$p = f_\theta(g, c) : \mathbb{R}^D \times \mathbb{R}^K \rightarrow \mathbb{R}^3, \quad (1)$$

where θ are learnable parameters of the share-weight MLP. When D is 2 or 1, FoldingNet can be considered as a deep parametric surface/curve as analogous to a NURBS surface/curve, where θ are knot vectors defining basis functions, c control points defining the shape of control mesh, and g the spline parameter. Varying the value of g will trace out the 3D surface/curve shape. The advantage of using FoldingNet than NURBS or other splines is that FoldingNet enables better and more flexible data-driven learning of the shape, while knot vectors in NURBS can not be optimized easily in surface fitting.

Although FoldingNet already has some desirable properties, there are still several facts in the original FoldingNet decoder that calls for improvement for more effective applications in our framework:

- Because $D \ll K$, $[g_i, c]$ is dominated by the same K -dimensional vector c , which slows down the learning.
- The parameter grid G is sampled on a 2D square. However, a soft robot could potentially be of any shape. Therefore, always using a 2D square as the parameter grid could also slow down the learning, and reduce the expressive power of the network.

- There is only one decoder in the original FoldingNet. However, it is sometimes desirable to be able to sense the complete shape of a soft robot. Due to possible self-occlusions of a soft robot, we need to use multiple 3D cameras to obtain the complete shape from different views. But multiple 3D cameras such as Kinect may interfere with each other when they operate simultaneously. One way to circumvent this interference problem is to collect data respectively from each camera with others turned off. Therefore, each individual ground truth 3D shape is only a partial view of the full shape. To get a complete 3D shape, we have to use multiple decoders.

Due to the above reasons, we propose to improved FoldingNet decoder formally from equation 1 to the following:

$$p = f_{\theta}(g, c) = f_{\theta}(l_{\phi}(g) + c), \quad (2)$$

realizing the following improvements (see Figure 2):

- **Learned constant biasing.** Instead of concatenating the grid points G to $\mathbb{1}_M c$, each D -dimension grid point in g_j is first mapped to K -dimension as a learned constant bias $b_j := l_{\phi}(g_j) \in \mathbb{R}^K$ using another share-weight MLP $l_{\phi} : \mathbb{R}^D \rightarrow \mathbb{R}^K$, then added with c . This will help the training process converge faster and enable a smaller network with less parameters. As shown in Figure 3, this modification leads to a lighter weight network with 50% parameter reduction yet still converges faster.
- **Deforming from prototype.** Instead of always sample from a 2D square for the parameter grid, we propose to use a prototype shape, and increase the dimension of D from 2 to 3. The prototype shape here is a 3D mesh model that is close to the static shape of the soft robot at its zero-state. It could be a cylinder, sphere, cube, or even a rough CAD model of the robot.
- **Multiple decoders.** Instead of using only one decoder, we enable the use of multiple different decoders (each with its own learnable parameters θ, ϕ). Each decoder corresponds to a particular view and is responsible to predict the partial 3D shape observed by the 3D camera from that view, given the same latent code c . In the training process, if the point cloud comes from a particular depth camera, then only the encoder weights and the weights of the corresponding decoder are updated. Due to this asynchronous multi-view ground truth, the original Chamfer Distance ($D_{\text{Chamfer}}\{\cdot, \cdot\}$) based loss [21] has to be modified as follows. If there are C views, and there are C_i point clouds collected from the i -th view, our new loss function is:

$$L(\psi, \{\theta_i, \phi_i\}) = \sum_{i=1}^C \frac{1}{C_i} \sum_{j=1}^{C_i} D_{\text{Chamfer}}\{\hat{P}_j^i, P_j^i(\psi, \theta_i, \phi_i)\}, \quad (3)$$

where P_j^i is the j -th predicted point cloud of the i -th view, and \hat{P}_j^i is the corresponding ground truth point cloud. ψ are the parameters of encoder h_{ψ} , and θ_i, ϕ_i

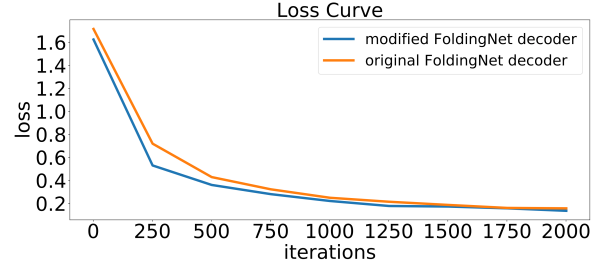


Fig. 3. Loss curves of the original FoldingNet decoder and our modified one on the same training set shows that the modified decoder learns faster. Note that the original decoder has 1.05×10^6 parameters, while the modified decoder only has 0.54×10^6 parameters.

are the parameters of the decoder MLPs f_{θ} and l_{ϕ} corresponding to the i -th view. The Chamfer distance [21] between point cloud P_a and P_b is defined as:

$$D_{\text{Chamfer}}(P_a, P_b) = \frac{1}{N_a} \sum_{a \in P_a} \min_{b \in P_b} \|a - b\| + \frac{1}{N_b} \sum_{b \in P_b} \min_{a \in P_a} \|b - a\|, \quad (4)$$

where N_a and N_b are numbers of points in point clouds P_a and P_b respectively.

IV. VISION-BASED SENSOR DESIGN FOR SOFT ROBOTS

Our data collection system is shown in Figure 4. We embed a camera inside the soft robots on the one end, in order to track the deformation (see Figure 4 right). The soft robot is fixed on the table, and 2 Kinect cameras are arranged on two opposite sides of the robot to capture its full 3D shapes. These shapes are used as the ground truth. We also paint some patterns on the robots to increase the visibility of the deformation. The patterns are made in multiple colors and the shapes of checkerboards, and each grid has a length of around 1 to 3 cm. The design of the pattern aims at making the visual cue caused by the robot deformation more distinguishable. Currently the shape and color arrangement of the patterns are randomly decided. We aim to investigate its influence to our method in the future, which could potentially further increase our computational efficiency.

We set up the sensing system on 4 different robots: a latex twisting balloon (Figure 5), a silicone cylindrical balloon modified from elastomeric origami [7] (Figure 6), a PneuNets [8] (Figure 7(a)) and a fiber reinforcement actuator [9] (Figure 7(b)). For the latex balloon and the fiber reinforcement actuator, we manually paint the arbitrary patterns on the surface of the robot. For the silicone balloon modified from elastomeric origami, we print a paper with arbitrary patterns and stick it inside the robot. The PneuNets design has limited inside space for the air channel, which is not desirable for the internal camera, so that we place the camera outside the robot at the end. Latex balloon, PneuNets and fiber reinforcement actuator are controlled by an air pump to inflate and deflate, which will cause them either to expand and shrink in overall

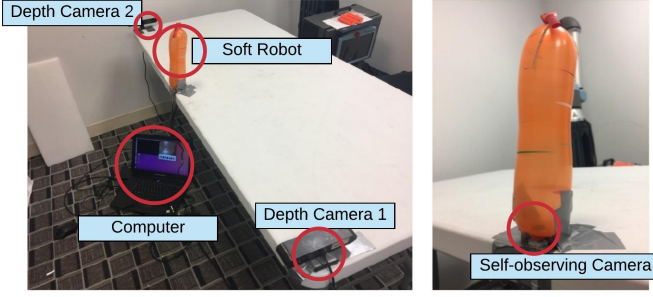


Fig. 4. Our data collection system.

size (the latex balloon), or bend into one direction (the PneuNet and fiber reinforcement actuator).

A. Collecting ground truth shapes with 2 RGBD cameras

The arrangement of 2 RGBD cameras (or possibly more in the future) aims at building a full 3D shape of the robot, regardless of the occlusion from the single view. Because multiple Kinects' IR cameras will interfere with each other, they cannot operate simultaneously, as explained in section III-B. Meanwhile, each Kinect camera can be easily synchronized with the embedded self-observing camera by connecting them to the same laptop, so we can collect a ground truth shape \hat{P}_n^i for the i -th Kinect camera paired with a self-observing image S_n .

Although we cannot synchronize the two views of Kinect camera, we have to obtain their relative 6 DOF poses, in order to register the two partial view into one common frame. This registration of the two Kinect cameras are performed prior to data collection. Iterative Closest Point (ICP) based registration from static background points cannot be applied due to the lack of overlapping background points from the two opposite-looking Kinect cameras. Therefore we developed a registration procedure by capturing multiple frames of synchronized point clouds of a thin plane moving between the two Kinect cameras (note that the IR interference is no longer an issue in this case because the thin board blocks the IR illumination from the opposite Kinect camera). Then we segment the thin board's points across all the frames for each Kinect camera respectively. Then the resulting two sets of planar points (the first two column on the bottom of Figure 8) can be registered by ICP (the registered results show on the last column of Figure 8), providing the desired relative pose between the two Kinect cameras.

During the data collection, we segment the point cloud of the target soft robot by cropping on the depth images with a fixed bounding box and depth filtering. We always randomly sample 2048 points from the segmented point cloud on each frame to build the ground truth dataset.

B. Data collection with soft robots

We collect self-observing images and 3D shape data of 4 different soft robots as mentioned above. Active and passive

TABLE I
DEFORMATION AND ACTUATION TYPES

	Latex balloon	Silicone balloon	PneuNets	Fiber re.
Def.	expansion & bend	local pressing	bend	bend
Act.	pump & rope	None	pump	pump

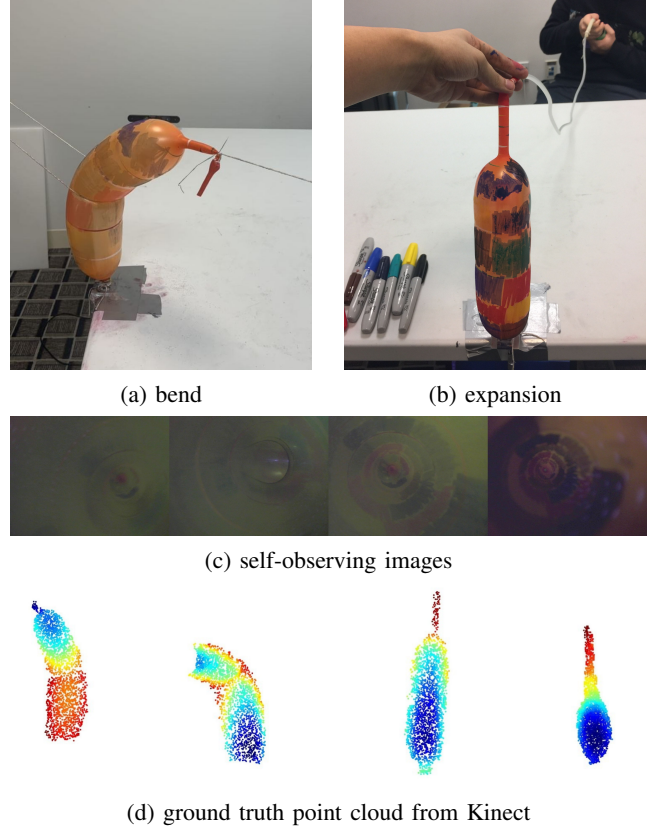


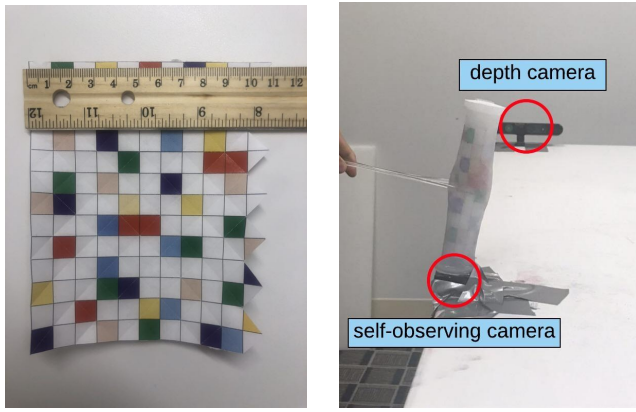
Fig. 5. Data collection for the latex balloon.

deformation are applied on these robots. With the latex twisting balloon, we inflate and deflate it to change the volume. Besides, we also pull the latex balloon with ropes to conduct bending deformation. With the silicone cylindrical balloon, we deform it by clamping it with a transparent chopstick (transparency to avoid Kinect camera capturing the shape of the chopstick). With PneuNets and the fiber reinforcement actuator, we inflate them to make them bent. Examples of the data collection process are shown in Figure 5, 6 and 7. Deformation and actuation types are depicted in Table I.

V. EXPERIMENTAL RESULTS

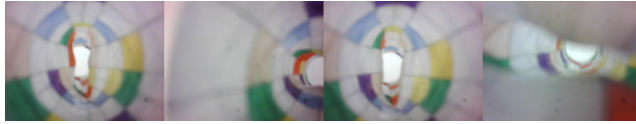
This section reports the accuracy and the computational speed of the 3D reconstruction neural network. The accuracy is measured by the Chamfer distance between the predicted point clouds to the ground truth. We also analyze the influence of hyper-parameters, like the resolution of input images and dimension of latent space, with respect to the prediction accuracy.

All experiments were run on a desktop computer with Intel i9-7900X CPU, NVIDIA TITAN Xp GPU and 64GB RAM. We use PyTorch [26] to implement the neural networks.

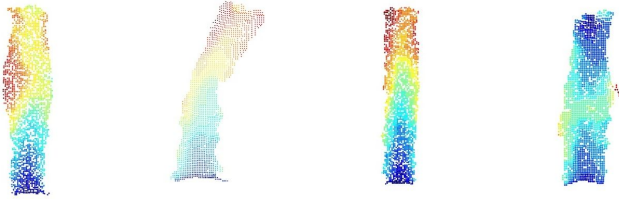


(a) random pattern

(b) passive deformation

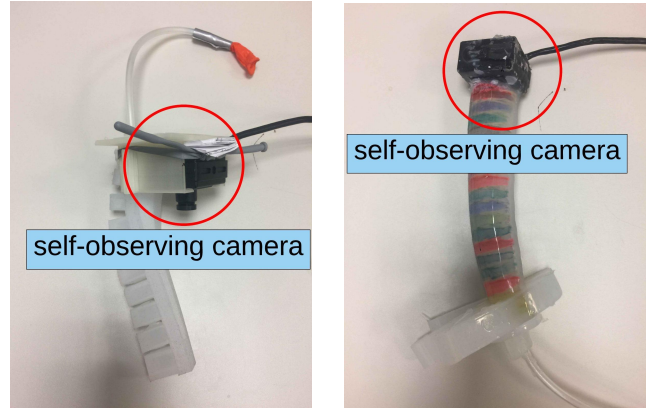


(c) self-observing images



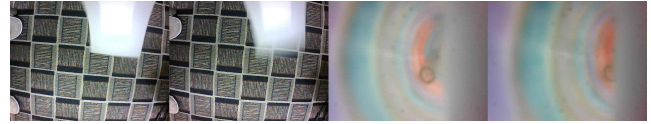
(d) ground truth point cloud from Kinect

Fig. 6. Data collection for the silicone cylindrical balloon.

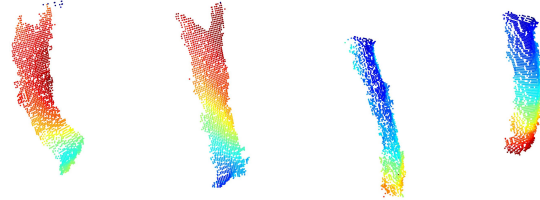


(a) PneuNets

(b) fiber reinforcement



(c) self-observing images



(d) ground truth point cloud from Kinect

Fig. 7. Data collection for PneuNets and fiber reinforcement actuator.

A. Training the neural network

Data Preprocessing. For a more effective representation of the neural networks, we normalize the point clouds in the depth images, either the ground truth ones from RGBD camera, or the output of the neural networks, into $[-1, 1]$. The image from the embedded camera is down-sampled to 224×224 .

Mapping Images to Latent Space As mentioned above, our proposed method can take advantage of both learned and hand-crafted latent space. The latex balloon dataset contains more variation in terms of deformation types than the other three datasets. Therefore, for the latex balloon dataset, we apply ResNet18[27] to learn a latent code. And for the other three datasets with simpler motions, we directly down-sample the images to 14×14 with 3 color channels and stretch the down-sampled images to $14 \times 14 \times 3 = 588$ dimensional vectors. These vectors are directly used as latent codes.

Training Settings. Training-testing division is set to 10:1. For the active deformation experiment, we collect a dataset of 20,000 samples for training and 2,000 for testing with the basic balloon setting, and 10,000 training data and 1,000 testing data for each other robot.

Adam optimizer with 0.0001 learning rate is employed, and the batch size is set to 16. All training processes in this paper terminate at the 200th epoch.

Prototype for Decoding. As mentioned above, using a pro-

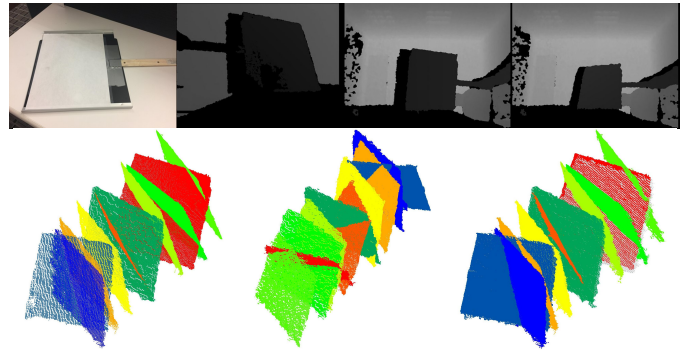


Fig. 8. **Registration of two Kinect cameras:** the first column of the top row is the thin board we used for registering the two opposite-looking Kinect cameras. The board moves in between the two cameras with different poses, and the depth images (the rest of the top row) are taken by the two depth cameras simultaneously. Then the points on the board are selected for the ICP registration. The bottom row shows the planar points observed from the two Kinect cameras (column 1 and 2) and the registered result (column 3). Points of the same color come from the same frame of a particular Kinect camera.

totype close to the shape of the soft robot as the point grid for decoding can accelerate the convergence of the training. In the experiments, half cylinder is used as the prototype for decoders of each view. It has 45 layers of points distributed equally from -1 to 1 in y-direction along the axis of the cylinder, where in each layer 45 points are uniformly distributed on a half circle with radius 1 (unitless) (see Figure 10).

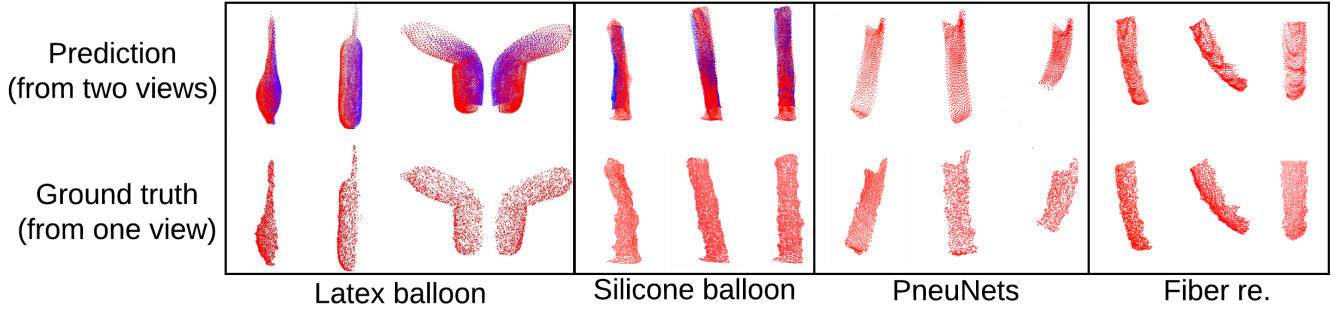


Fig. 9. **Qualitative results on various soft robots.** From left to right: latex balloon shrink/expand/left-bend/right-bend, silicone balloon local deformation, PneuNets bend, and fiber reinforcement actuator bend. The top row illustrates our predictions and the bottom row illustrates the ground truth. Red and blue points are predicted from two different views respectively. Although the ground truth is collected from two views separately, our multi-view decoders are able to predict points from two views simultaneously.

TABLE II
POINT CLOUD PREDICTION ERROR

	Length (mm)	Abs. Err. (mm)	Rel. Err. (%)
Latex balloon	400	5	1.2
Silicone balloon	150	4	2.7
PneuNets	170	7	4.1
Fiber re.	200	8	4.0

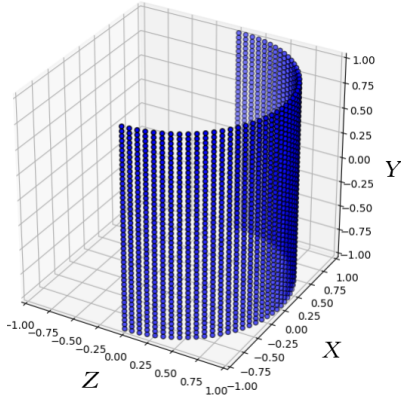


Fig. 10. **The prototype shape**, i.e., the grid points G , used in our experiments. A soft robot's 3D shape is deformed from this shape depending on a latent code estimated from a self-observing image.

B. Shape reconstruction accuracy

Table II shows absolute and relative errors in the test. Absolute error is defined by the average Chamfer distance between predicted point clouds and ground truth point clouds in the test set. Relative error is the absolute error divided by the robot's length. Errors of all experiments are below 5%. Possible reason could be due to limitation of accuracy of the depth camera. If there is a higher-accuracy 3D sensor, we believe that our proposed method can obtain better performance. The proposed method shows very high accuracy in terms of similarity of predicted point cloud to the ground truth. Figure 9 depicts some examples of predicted point cloud with the ground truth. Note that the ground truth point cloud has only one view, but the predicted point cloud has two views and they are painted in to different colors.

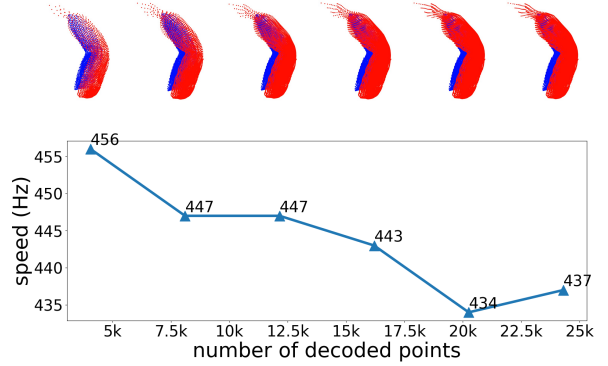


Fig. 11. **Computational speed vs. number of decoded points:** the top images show the shape reconstruction results decoded with 4050, 8100, 12150, 16200, 20250, 24300 points respectively.

C. Computational speed

Since the decoder of FoldingNet is not limited to the number of points it decodes, it is necessary to study on how increasing the number of points decoded influences the computation speed. Figure 11 shows the computational speed vs. the number of points decode. Our method reveal its high efficiency. With 400% increase in number of points, the speed only decreases by 4.1%. This result demonstrates that our method can reconstruct the 3D shape with higher resolution (in terms of number of points) than the ground truth, without significantly sacrificing speed.

D. Hyper-parameter analysis

We study the choice of hyper-parameters to obtain a better understanding of our method, and to test the adaptability of our method to resource-limited situations.

Resolution of input images. The original CNN's input image resolution is 224×224 . In this experiment, images are first down-sampled to 56×56 , 14×14 and 4×4 . The dimension of latent space K is kept at 512. Figure 12 shows the quantitative and qualitative evaluation on the influence of reducing the image resolution. The model can provide reasonable prediction even when the image size reduces to only 56×56 . This result indicates that our method can tolerate

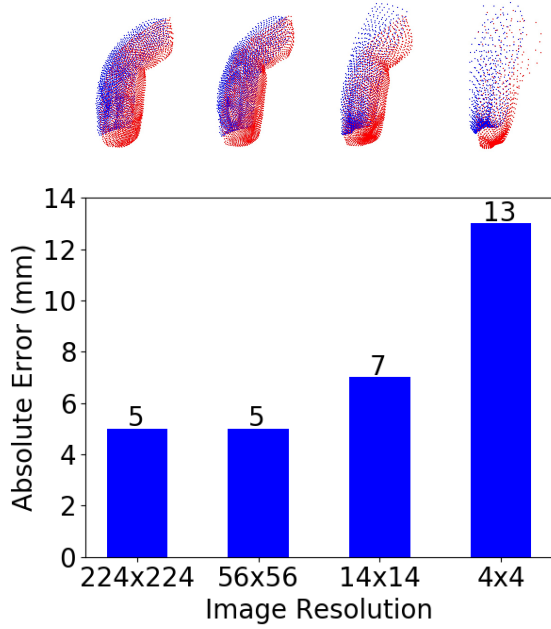


Fig. 12. **Accuracy vs. self-observing image resolution.** The top row from left to right shows the corresponding 3D shapes reconstructed from self-observing images.

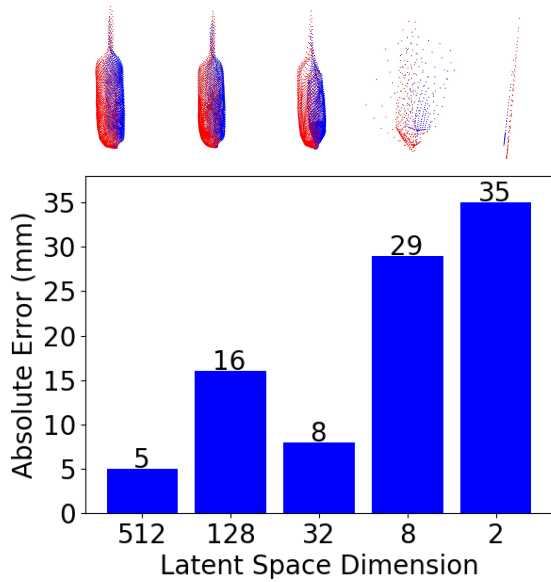


Fig. 13. **Accuracy vs. latent space dimension.** The top row from left to right shows the corresponding 3D shapes reconstructed from self-observing images.

low-resolution images, which sometimes is the only choice of self-observing signals on robot, due to limits of cost, space, installation difficulty, etc.

Dimension of latent space. ResNet18 can encode the input image into a 512 dimensional vector, so we first use the 512-d vector as of the latent vector. To explore if the dimension of the latent space can be further reduced, an additional MLP is added after ResNet18 to change the latent vector dimension

from 512 to K . We experiment with the K of 128, 32, 8, and 2 respectively while keeping the image size as 224×224 . Figure 13 shows the evaluation of different dimensions of the latent space. The result shows that when K is lower than 512, there is a significant decrease in the prediction accuracy. This high dimensional state space is justified due to the highly nonlinear nature of soft robots, although still much more manageable than the theoretical infinite degrees of freedom of soft robots.

VI. CONCLUSION AND DISCUSSION

In this paper, we propose a vision-based sensing system to measure the soft robots' real-time 3D shapes, which is their core proprioception and can be used for closed-loop control in precise tasks. The system uses a CNN to encode the input images from the internal cameras into latent codes, and then train a decoder neural network to reconstruct the 3D shapes of the robot from the latent codes. For the training and validation purpose, we also build a dual-Kinect system to get the ground truth shapes of the robots. Experimental results show that our system can provide an accurate and efficient measurement of 4 different soft robots' 3D shapes. Compared to the existing measuring methods for soft robot preconception, our method well measures the full 3D models of the robots under complicated loading conditions, and can be easily applied to different designs of the robots, especially with a minimum request in hardware fabrication.

The neural networks we proposed for dimension reduction for the soft robot, i.e. the representation into a latent space, has more potential applications related to soft robots. For example, instead of using cameras, other embedded sensors can provide the input for the network as well. The latent code, which is a neat description of the robots' internal state, can also be used for other goals, such as serving as the state for control or motion planning for the soft robots. At the same time, we are also interested to explore the performance of our system on other designs of the soft robots. We will further explore those research directions in the future.

REFERENCES

- [1] Yaoqing Yang, Chen Feng, Yiru Shen, and Dong Tian. Foldingnet: Interpretable unsupervised learning on 3d point clouds. *arXiv preprint arXiv:1712.07262*, 2017. 1, 2, 3
- [2] CK Harnett. Flexible circuits with integrated switches for robotic shape sensing. In *Sensors for Next-Generation Robotics III*, volume 9859, page 98590I. International Society for Optics and Photonics, 2016. 1
- [3] Haojian Jin, Jingxian Wang, Zhijian Yang, Swarun Kumar, and Jason Hong. Wish: Towards a wireless shape-aware world using passive rfids. In *Proceedings of the 16th Annual International Conference on Mobile Systems, Applications, and Services*, pages 428–441. ACM, 2018. 1
- [4] Michael Wessely, Theophanis Tsandilas, and Wendy E Mackay. Shape-aware material: Interactive fabrication with shapeme. In *The 31st Annual ACM Symposium on*

- User Interface Software and Technology*, pages 127–139. ACM, 2018. 1
- [5] G Runge, M Wiese, L Günther, and A Raatz. A framework for the kinematic modeling of soft material robots combining finite element analysis and piecewise constant curvature kinematics. In *Control, Automation and Robotics (ICCAR), 2017 3rd International Conference on*, pages 7–14. IEEE, 2017. 1
- [6] Zhongkai Zhang, Jeremie Dequidt, Alexandre Kruszewski, Frederick Largilliere, and Christian Duriez. Kinematic modeling and observer based control of soft robot using real-time finite element method. In *Intelligent Robots and Systems (IROS), 2016 IEEE/RSJ International Conference on*, pages 5509–5514. IEEE, 2016. 1
- [7] Ramses V Martinez, Carina R Fish, Xin Chen, and George M Whitesides. Elastomeric origami: programmable paper-elastomer composites as pneumatic actuators. *Advanced functional materials*, 22(7):1376–1384, 2012. 2, 4
- [8] Bobak Mosadegh, Panagiotis Polygerinos, Christoph Keplinger, Sophia Wennstedt, Robert F Shepherd, Unmukt Gupta, Jongmin Shim, Katia Bertoldi, Conor J Walsh, and George M Whitesides. Pneumatic networks for soft robotics that actuate rapidly. *Advanced functional materials*, 24(15):2163–2170, 2014. 2, 4
- [9] Panagiotis Polygerinos, Zheng Wang, Johannes TB Overvelde, Kevin C Galloway, Robert J Wood, Katia Bertoldi, and Conor J Walsh. Modeling of soft fiber-reinforced bending actuators. *IEEE Transactions on Robotics*, 31(3):778–789, 2015. 2, 4
- [10] Oliver Glauser, Daniele Panozzo, Otmar Hilliges, and Olga Sorkine-Hornung. Deformation capture via self-sensing capacitive arrays. *arXiv preprint arXiv:1804.04013*, 2018. 2
- [11] IM Van Meerbeek, CM De Sa, and RF Shepherd. Soft optoelectronic sensory foams with proprioception. *Science Robotics*, 3(24):eaau2489, 2018. 2
- [12] Jennifer L Molnar, Ching-An Cheng, Lucas O Tiziani, Byron Boots, and Frank L Hammond. Optical sensing and control methods for soft pneumatically actuated robotic manipulators. In *IEEE International Conference on Robotics and Automation (ICRA)*, pages 1–8. IEEE, 2018. 2
- [13] Hongbo Wang, Massimo Totaro, and Lucia Beccai. Toward perceptive soft robots: Progress and challenges. *Advanced Science*, 5(9):1800541, 2018. 2
- [14] Nicola J Ferrier and Roger W Brockett. Reconstructing the shape of a deformable membrane from image data. *The International Journal of Robotics Research*, 19(9):795–816, 2000. 2
- [15] Kazuto Kamiyama, Kevin Vlack, Terukazu Mizota, Hiroyuki Kajimoto, K Kawakami, and Susumu Tachi. Vision-based sensor for real-time measuring of surface traction fields. *IEEE Computer Graphics and Applications*, 25(1):68–75, 2005. 2
- [16] Craig Chorley, Chris Melhuish, Tony Pipe, and Jonathan Rossiter. Tactile edge detection. In *Sensors, 2010 IEEE*, pages 2593–2598. IEEE, 2010. 2
- [17] Akihiko Yamaguchi and Christopher G Atkeson. Implementing tactile behaviors using fingervision. In *IEEE-RAS 17th International Conference on Humanoid Robotics (Humanoids)*, pages 241–248. IEEE, 2017. 2
- [18] Wenzhen Yuan, Siyuan Dong, and Edward H Adelson. Gelsight: High-resolution robot tactile sensors for estimating geometry and force. *Sensors*, 17(12):2762, 2017. 2
- [19] Christopher B Choy, Danfei Xu, JunYoung Gwak, Kevin Chen, and Silvio Savarese. 3d-r2n2: A unified approach for single and multi-view 3d object reconstruction. In *European conference on computer vision*, pages 628–644. Springer, 2016. 2
- [20] Xingyuan Sun, Jiajun Wu, Xiuming Zhang, Zhoutong Zhang, Chengkai Zhang, Tianfan Xue, Joshua B Tenenbaum, and William T Freeman. Pix3d: Dataset and methods for single-image 3d shape modeling. In *Proceedings of the IEEE Conference on Computer Vision and Pattern Recognition*, pages 2974–2983, 2018. 2
- [21] Haoqiang Fan, Hao Su, and Leonidas J Guibas. A point set generation network for 3d object reconstruction from a single image. In *Proceedings of the IEEE conference on computer vision and pattern recognition*, pages 605–613, 2017. 2, 4
- [22] Rıza Alp Güler, Natalia Neverova, and Iasonas Kokkinos. Densepose: Dense human pose estimation in the wild. In *Proceedings of the IEEE Conference on Computer Vision and Pattern Recognition*, pages 7297–7306, 2018. 2
- [23] Jiajun Wu, Chengkai Zhang, Tianfan Xue, William T Freeman, and Joshua B Tenenbaum. Learning a probabilistic latent space of object shapes via 3d generative-adversarial modeling. In *Advances in Neural Information Processing Systems*, pages 82–90, 2016. 2, 3
- [24] Wei Zhuang, Guangkai Sun, Hong Li, Xiaoping Lou, Mingli Dong, and Lianqing Zhu. Fbg based shape sensing of a silicone octopus tentacle model for soft robotics. *Optik*, 165:7–15, 2018. 3
- [25] Charles R Qi, Hao Su, Kaichun Mo, and Leonidas J Guibas. Pointnet: Deep learning on point sets for 3d classification and segmentation. *Proc. Computer Vision and Pattern Recognition (CVPR), IEEE*, 1(2):4, 2017. 3
- [26] PyTorch. <https://pytorch.org/>. 5
- [27] Kaiming He, Xiangyu Zhang, Shaoqing Ren, and Jian Sun. Deep residual learning for image recognition. In *Proceedings of the IEEE conference on computer vision and pattern recognition*, pages 770–778, 2016. 6